

LA-UR-15-23495 (Accepted Manuscript)

Characterization and comparative analysis of the tensile properties of five tempered martensitic steels and an oxide dispersion strengthened ferritic alloy irradiated at 295 °C to 6.5 dpa

Maloy, Stuart Andrew
Saleh, Tarik A.
Anderoglu, Osman
Romero, Tobias J.
Odette, G. Robert
Yamamoto, Takuya
Li, S.
Cole, James
Fielding, Randall

Provided by the author(s) and the Los Alamos National Laboratory (2016-05-24).

To be published in: Journal of Nuclear Materials

DOI to publisher's version: 10.1016/j.jnucmat.2015.07.039

Permalink to record: <http://permalink.lanl.gov/object/view?what=info:lanl-repo/lareport/LA-UR-15-23495>

Disclaimer:

Approved for public release. Los Alamos National Laboratory, an affirmative action/equal opportunity employer, is operated by the Los Alamos National Security, LLC for the National Nuclear Security Administration of the U.S. Department of Energy under contract DE-AC52-06NA25396. Los Alamos National Laboratory strongly supports academic freedom and a researcher's right to publish; as an institution, however, the Laboratory does not endorse the viewpoint of a publication or guarantee its technical correctness.

Characterization and Comparative Analysis of the Tensile Properties of Five Tempered Martensitic Steels and an Oxide Dispersion Strengthened Ferritic Alloy Irradiated at $\approx 295^{\circ}\text{C}$ to ≈ 6.5 dpa

S.A. Maloy*, T. A. Saleh, O. Anderoglu, T.J. Romero, LANL

G.R. Odette, T. Yamamoto, S. Li, UCSB

J. Cole, R. Fielding, INL

*corresponding author's e-mail: maloy@lanl.gov

Abstract

Tensile test results at 25 and 300°C on five 9-12Cr tempered martensitic steels and one 14Cr oxide dispersion strengthened alloy, that were side-by side irradiated to 6.5 dpa at 295°C in the Advanced Test Reactor (ATR), are reported. The engineering stress-strain curves are analyzed to provide true stress-strain constitutive $\sigma(\epsilon)$ laws for all of these alloys. In the irradiated condition, the $\sigma(\epsilon)$ fall into categories of: strain softening, nearly perfectly plastic and strain hardening. A range of increases in yield stress ($\Delta\sigma_y$) and reductions in uniform strain ductility (e_u) are observed, where the latter can be understood in terms of the alloy's $\sigma(\epsilon)$ behavior. Increases in the average $\sigma(\epsilon)$ in the range of 0-10% strain are smaller than the corresponding $\Delta\sigma_y$, and vary more from alloy to alloy. The data are also analyzed to establish relations between $\Delta\sigma_y$ and coupled changes in the ultimate stresses as well as the effects of both test temperature and the unirradiated yield stress (σ_{yu}). The latter shows that higher σ_{yu} correlates with lower $\Delta\sigma_y$. In five out of six cases the effects of irradiation are generally consistent with previous observations on these alloys. However, the particular heat of the 12Cr HT-9 tempered martensitic steel in this study has a much higher e_u than observed for earlier heats. The reasons for this improved behavior are not understood and may be microstructural in origin. However, it is noted that the new heat of HT-9, which was procured under modern quality assurance standards, has lower interstitial nitrogen than previous heats. Notably there is a general relation between lower interstitial solute contents and improved ductility, and homogenous deformation, in broadly similar steels.

1. Introduction and Background

A key objective of the Fuel Cycle Research and Development Program is to qualify advanced, high burn-up (to 40%) fast spectrum reactor fuel and cladding systems that transmute minor actinides, thereby helping to close the nuclear fuel cycle [1]. The cladding pin must contain the fuel and fission products at an extremely high level of reliability. Thus the cladding alloy must be resistant to high dose irradiation damage, up to a maximum of 400 dpa, over prototypic fast reactor temperatures of 350 - 550°C , while in contact with the liquid metal coolant. In particular, cladding alloys must resist various irradiation degradation phenomena, like void swelling at intermediate temperatures (400 - 500°C) and reductions of ductility and fracture toughness, particularly at temperatures below 400°C .

It is well established that so-called ferritic/martensitic alloys have much better resistance to void swelling than austenitic alloys. In the former case incubation doses for significant swelling in fast reactor

neutron environments of up to ≈ 200 dpa have been observed and are projected to be higher in some cases [2-7]. Note, that the swelling incubation dpa decreases in the presence of high quantities of helium, roughly linearly with an increasing He/dpa ratio [5, 6, 8, 9]. However, compared to austenitic steels, the degradation of toughness and ductility¹ at irradiation temperatures below $\approx 400^\circ\text{C}$ may be as, or even more, severe, especially in the presence of large quantities of helium [3-6, 10, 11]. There is a large body of literature on irradiation effects on the tensile properties for a broad alloy class that are referred to here as tempered martensitic steels (TMS) containing 8-12%Cr [3, 5, 6, 10-13]. The corresponding databases span decades of research, a wide variety of applications (fission, fusion and accelerator based technologies) and a range of alloys in the broad TMS class. More recently, an emerging database on the effects of irradiation on the tensile properties of so-called oxide dispersion strengthened (ODS) steels has been developing, including for ODS nanostructured ferritic alloy (NFA) variants [5, 11, 12].

However, in their raw form, tensile test engineering stress-strain data $[s(e)]$ – see below] provide only part of the constitutive information needed for reactor design and in-service safety assessments. For example, designs may limit nominal component stresses to a fraction of the ultimate engineering tensile stress, s_{uts} , and a minimum uniform engineering strain ductility, e_u . However, more quantitative designs and detailed safety assessments, typically based on the finite element method (FEM) code analysis, require true effective stress-effective strain constitutive laws, $\sigma(\epsilon)$.

There is a modest, but significant, body of published results on irradiation effects on Charpy V-notch transition temperature shifts and a much smaller database on fracture master curve toughness shifts, ΔT_o [3, 5, 6, 10-14]. The irradiation induced changes in the fracture and constitutive properties are highly inter-related. For example, at lower irradiation temperatures the ΔT_o are primarily caused by, and can be related to, irradiation hardening, typically characterized by the change in yield stress, $\Delta\sigma_y$ [5, 6, 10, 14-16]. However, it has been shown that the change in the true flow stress between 0 and 10% plastic strain, $\Delta\sigma_{10}$, is a better measure of hardening to relate to toughness temperature shifts [17]. In the hardening dominated regime, $\Delta T_o \approx 0.7\Delta\sigma_{10}$, in units of $^\circ\text{C}$ and MPa [5, 6, 10, 14-17]. Finally we note that for FEM studies, fracture toughness data must account for cracked body size and geometry effects in a way that is very sensitive to the alloy's constitutive law, $\sigma(\epsilon)$ [14-16, 18-20].

Here we focus on irradiation effects on $\sigma(\epsilon)$ constitutive laws derived from simple tensile tests carried out on specimens irradiated side-by-side. In spite of the large body of irradiated tensile test results, there has been remarkably little corresponding analysis of this collective database, like deriving $\sigma(\epsilon)$ from measured $s(e)$, assessing, understanding and modeling the effects of alloy type, composition and starting microstructure on $\sigma(\epsilon)$ and in evaluating the inter-relationship between various tensile properties in both the unirradiated and irradiated condition. This study is aimed at addressing some of these unmet opportunities.

2. Tensile Test Engineering $s(e)$ Data and $\sigma(\epsilon)$ Constitutive Laws: Objectives

¹ It is very important to note that fracture toughness and ductility are not the same properties, although they are often confused.

Standard tensile tests directly provide data on engineering stress and strain, $s(e)$, defined in the usual way: “ s ” given by load divided by the initial cross section area and “ e ” given by the change in gauge length divided by its original length. Tensile properties are usually simply characterized by the engineering yield stress $s_y \approx \sigma_y$, the ultimate stress (s_{uts}) the uniform elongation (e_u) at the onset of necking, the total elongation (e_t) and the reduction in area (RA), both at specimen rupture. Note, the so-called ductility and post yield stress measures are not true material properties, since they depend on the gauge section cross-section shape and dimensions. It is trivial to convert $s(e)$ to $\sigma(\epsilon)$ up to the point of necking². However, due to typically very low e_u after irradiation, tensile test $s(e)$ that undergo nearly immediate necking, cannot directly provide post-yielding $\sigma(\epsilon)$. Plastic strains increase rapidly to high values in the necked region undergoing large geometry changes, where continued deformation occurs under complex tri-axial stress states³. However, as described below, $s(e)$ curves can be used to derive $\sigma(\epsilon)$ up to large ϵ by iterative FEM calculations.

Increasing irradiation hardening is also often⁴ accompanied by a greater degree of internal mesoscale flow localization in high strain, deformation softened shear bands [21-23]. While flow localization plays a role in reductions in $d\sigma(\epsilon_u)/d\epsilon$, the irradiated e_u (or ϵ_u) is more generally controlled by the classical Considere’s plastic instability criterion given by

$$d\sigma(\epsilon)/d\epsilon < \sigma(\epsilon). \quad [1]$$

Thus increases in $\sigma(\epsilon)$ and decreases in $d\sigma(\epsilon)/d\epsilon$ combine to reduce ϵ_u .

In this short paper we focus on the effects of irradiation to about ≈ 6.5 dpa at $\approx 295^\circ\text{C}$, on the tensile properties of five 8-12Cr TMS’s and one ODS alloy. These irradiation conditions result in large increases in the yield stress (σ_y) and flow stress [$\sigma(\epsilon)$], $\Delta\sigma_y$ and $\Delta\sigma(\epsilon)$, up to several hundred MPa. The strength increases coincide with large reductions in the e_{uu} to e_{ui} , and more modest reductions in both e_{tu} and e_{ti} , and corresponding post necking total strains ($\epsilon_{tu} - \epsilon_{uu}$) to ($\epsilon_{ti} - \epsilon_{ui}$). Here the subscripts u and i designate the unirradiated and irradiated conditions, respectively. The irradiated tensile test rupture process remains ductile and occurs by micro-void nucleation, growth and coalescence. Thus the major structural degradation impact of these irradiation conditions is a severe reduction of plastic strain at the maximum load under tensile test conditions⁵, as characterized by the uniform elongation, e_{ui} .

Here we contrast and analyze the tensile properties of the TMS and an ODS alloy that were irradiated side-by-side in the Nuclear Science Users Facility (NSUF) UCSB ATR-1 irradiation experiment. Four of the five normalized and tempered TMS alloys contain $\approx 8\text{-}9\%$ Cr, while the other contains $\approx 12\%$ Cr. The ODS alloy is a 14% Cr nearly fully ferritic stainless steel (MA957) that lies outside the Fe-Cr γ -loop. This fine

² For uniformly deforming gauge sections, $\sigma(\epsilon) = s(e)(1+e)$ and $\epsilon = \ln(1+e)$

³ The $\sigma(\epsilon)$ derived from tensile tests are assumed to represent effective stress and strain, that can be used under multi-axial loading conditions. Modeling plastic deformation also requires a proper description of the governing flow potential (like J_2 flow theory) and associated flow-hardening rules.

⁴ Flow localization does not always occur, especially under precipitation dominated hardening conditions. Localization is most often associated with hardening dominated by dislocation loops.

⁵ Note low strain plastic instabilities are a characteristic of the tensile loading geometry and, for example, do not occur under bending or compression loading.

grained ODS variant, also known as a NFA since it also contains an ultrahigh density of nm-scale complex oxide precipitates, is characterized by high strength, substantial tensile ductility and remarkable resistance to irradiation damage [5, 6, 10, 15, 24, 25].

The main objectives of this work include addressing the following:

To derive true stress-strain constitutive $\sigma(\epsilon)$ laws from the engineering stress strain $s(e)$ curves; only the results of this analysis are shown here.

To determine how the hardening and ductility loss trends inter-compare for the 9Cr TMS, the 12Cr TMS and the 14Cr ODS alloy in the side-by-side ATR-1 irradiation, and specifically how these properties relate to the alloy type, composition, as well as the unirradiated microstructure and properties.

To provide a basis to determine how the current ATR-1 results compare to those previously reported on the same, or similar, alloys; and how might the differences depend on finer details of the specific alloy heat, such as interstitial impurity compositions, as well as the unirradiated microstructures and properties. The latter objective primarily pertains to understanding the 12% Cr TMS and 14% Cr ODS that retain a high uniform strain capacity.

To establish relations between various alloy strength and ductility unirradiated properties and the corresponding irradiated property changes.

Four out of the five TMS alloys in the unique ATR-1 database behave in a generally expected manner as does the ODS alloy. However the 12Cr TMS, which is a new heat of HT9 steel, experiences a much smaller loss of uniform strain than the lower Cr alloys and previous heats of HT9. An analysis of the $s(e)$ and $\sigma(\epsilon)$ curves for the five TMS steels shows that the strain hardening rate is highest in the HT9 in both the unirradiated and irradiated condition, partly rationalizing the correspondingly higher ϵ_u . However, the reasons for the higher strain-hardening rate in the new HT9 heat are not yet fully understood. Higher strain-hardening rates are broadly related to microstructural features and length scales that mediate dislocation multiplication and annihilation rates; smaller length scales lead to higher hardening. However, the new heat of HT9 also has a much lower interstitial free N content than previous irradiated alloys. Notably, various studies have linked lower free N to higher ductility in Fe-based bcc alloys [26, 27].

3. Experimental Materials and Methods

The irradiation results reported here are from a large, multipurpose, University of California Santa Barbara led irradiation program carried out in the Advanced Test Reactor (ATR) at the Idaho National Laboratory (INL), as part of the ATR Nuclear Science Users Facility (NSUF) Program. One of many purposes of the UCSB ATR-1 experiment was to irradiate a large number of candidate structural alloys "side-by-side", at nearly identical temperatures and dpa, so that relatively direct comparisons of changes in their microstructures (not discussed here) and mechanical properties could be made, without many of the usual confounding factors encountered in analyzing results from different irradiations. Here

we focus on the results of tensile tests on five 9-12Cr TMS and one ODS alloy. The TMS include: HT-9 (H9), T91, F82H-IAEA (F2), NF616 (N6) and Eurofer97 (E9), where the (X#) notation indicates the compact alloy identification code used here. Note, while the other alloys have been irradiated in previous programs, this study included a new heat of HT9 produced by Metalwerks for the Fuel Cycle Research and Development (FCRD) program following a strict quality assurance program (NQA-1 standards). The measured alloy compositions and the TMS normalized and tempered heat treatments are also summarized in Table 1. This MA957 ODS alloy was processed by ball milling Y_2O_3 and elemental powders, followed by consolidation via hot extrusion at $\approx 1100^\circ\text{C}$ [28].

The irradiation was carried out in the A10 position in the ATR over a range of nominal temperatures from ≈ 290 to 750°C , and displacement damage doses from ≈ 1.7 to 6.5 dpa. A large number and wide range of specimen types (1375 in total) were contained in 32 UCSB designed sub-packets that optimized gas gap temperature control and minimized the corresponding specimen temperature uncertainties in the un-instrumented drop-in the ATR A10 position test train. The as run fluxes and fluences were calculated by the MCNP code, and varied over the 110 cm length of the 10 mm ID capsule, with a mid-core peak of flux $\approx 2.3 \times 10^{14}$ n/cm²-s ($E > 0.1$ MeV), corresponding to $\approx 3.5 \times 10^{-7}$ dpa/s, and a fluence $\approx 4 \times 10^{21}$ n/cm²/s. The temperatures were determined by detailed finite element thermal analyses conducted independently by both UCSB and INL. Further details on the UCSB ATR-1 experiment are described elsewhere [29]. The average irradiation conditions for the tensile specimens were $\approx 296^\circ\text{C}$ and 6.5 dpa. After irradiation and recovery from the test train in the Hot Fuel Examination Facility (HFEF) at INL, 12 sub-packets were transported in a Type A radioactive shipment to Los Alamos National Laboratory (LANL) for disassembly at the CMR Wing 9 hot cells. Individual specimens were ultrasonically cleaned in a degreaser followed by an acetone wash to remove any possible alpha contamination.

Table 1 Alloy Compositions (wt.%) and Heat Treatments

| Alloy | C | Cr | Mn | Ni | Si | Mo | Nb | V | W | O | N | P | S | Al | Cu | Co | Ti | Fe |
|-----------|------|-------|------|------|------|------|--------|-----|------|------|------|-------|--------|------|------|------|------|---------------|
| HT-9 | .201 | 12.49 | .41 | .60 | .28 | 1.07 | <.002 | .29 | .52 | .002 | .001 | .007 | <.0005 | .015 | .034 | - | - | Bal |
| Eurofer97 | .117 | 8.69 | .47 | .024 | .056 | .005 | <.002 | .20 | .82 | .003 | .023 | .004 | .002 | .009 | .023 | .011 | .006 | Bal |
| F82H | .093 | 7.89 | .16 | .026 | .12 | .005 | <.002 | .16 | 1.21 | .003 | .008 | .004 | .002 | .002 | .028 | .007 | .002 | Bal |
| NF616 | .108 | 9.71 | .46 | .064 | .056 | .47 | .043 | .20 | 1.22 | .003 | .060 | .007 | .001 | .003 | .035 | .015 | .003 | Bal |
| T91 | .052 | 9.22 | .46 | .18 | .24 | .96 | .063 | .24 | .013 | .002 | .057 | .016 | .001 | .009 | .087 | .021 | .002 | Bal |
| MA 957 | 0.02 | 13.57 | 0.07 | 0.10 | 0.03 | 0.30 | <0.002 | -- | -- | 0.22 | --- | 0.004 | 0.006 | 0.09 | 0.01 | --- | 0.98 | Bal |
| | | | | | | | | | | | | | | | | | | +0.25 Y2O3 |

Heat Treatments: HT9- 1040°C-1hr./air cool, 760°C 1hr./air cool; T91- 1040°C-1hr./air cool, 760°C 1hr./air cool; F82H IAEA- 1040°C-40min./air cool, 750°C 1hr./air cool; Eurofer97- 980°C-27min./air cool, 760°C 90min./air cool; NF616- Hot Rolled at 1025°C/air cool; 750°C-2hr./air cool

The tensile tests were carried out on sub-size SSJ-2 type specimens with a reduced gage length of 5 mm length, 1.2 mm width and 0.5 mm thickness. The tensile tests in the LANL CMR hot cells were carried out on an Instron 5567 screw driven test machine at a strain rate of 5×10^{-4} /s at both $\approx 25^\circ\text{C}$ and 300°C . The specimens were shoulder loaded to provide good alignment in tension. The thickness and width of the gage section of all the individual specimens were measured prior to testing. The elevated temperature tensile tests were performed in an inert argon atmosphere. In general, two irradiated tests were carried

out at 25°C, but only one test was conducted at 300°C. The redundant $s(e)$ curves at 25°C were very similar in all cases. A minimum of 2 tensile tests, and generally more, were carried out on the unirradiated controls at both 25°C and 300°C. The raw digitized load and load point displacement data were converted to nominal engineering stress-strain $s(e)$ curves used in the subsequent derivation of the $\sigma(\epsilon)$.

4. Analysis of true stress-strain $\sigma(\epsilon)$ constitutive laws

As noted previously, true stress-strain $\sigma(\epsilon)$ constitutive laws are needed for quantitative FEM, and other, analysis of the deformation and fracture in arbitrary geometries ranging from test coupons to complex in service structures, including under both normal operation and transient accident conditions. Developing $\sigma(\epsilon)$ for irradiated alloys from tensile tests is a challenge if they undergo a plastic instability and necking at very low uniform strains, e_u . Details of the iterative finite element analysis are described elsewhere[14, 30] , and will be the subject of a future publication that describes details about the derivation of the results shown in Section 5 including and analysis of large geometry changes (LGC) during necking. Briefly, the analysis reported here involves FEM simulation of the $s(e)$ curves based on input trial $\sigma(\epsilon)$ functions that are systematically modified until the predicted and measured $s(e)$ curves converge. The FEM simulations are carried out using the AbaqusTM package assuming isotropic J_2 -flow theory and using piecewise segmented input $\sigma(\epsilon)$ curves. Note the convergence requirement is only up to the strain marking a more rapid drop-off in the measured $s(e)$ curve (load), that is believed to be associated with the development of significant internal micro-void damage. We assume that internal damage and cracking can be ignored at lower strains, although this leads to some uncertainty in the derived $\sigma(\epsilon)$. Additional measurements of LGC and 3D strain maps, using techniques like digital image correlation, and tests in other geometries (like indentation hardness, bending and compression) can be used to verify further the iterative FE simulations, based on their self-consistency with the test observables [23].

5. Results

Here we use the method described in Section 4 to extract $\sigma(\epsilon)$ from engineering $s(e)$ curves. Figure 1 shows the results for both unirradiated and irradiated conditions on a consistent e or ϵ -scale up to 50%. Figures 1 (a to l) summarizes the results of the analysis for the six alloys in this study at 25°C (1a-f) and 300°C (1g-l), respectively. Each plot for a specific alloy shows the unirradiated (blue) and irradiated (red) $s(e)$ curves (heavy dashed lines) along with the corresponding derived $\sigma(\epsilon)$ curves (heavy dotted lines) and the converged FEM prediction of the $s(e)$ curve (light solid line). In this case limited LGC comparisons showed post-test images of the broken specimens are in good agreement with FE simulations in terms of the neck shapes and dimensions. Note, the diffuse necking behavior is in contrast to a paper in the literature for a A533B steel irradiated at low temperature ($< 100^\circ\text{C}$) that shows failure by a single large shear band that reaches the tensile specimen surfaces[31].

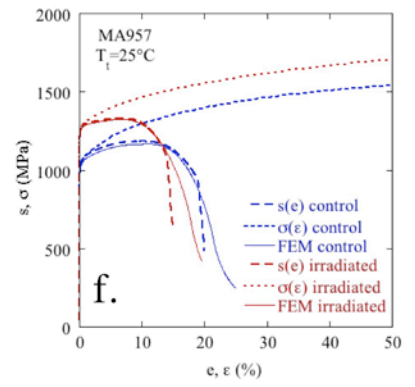
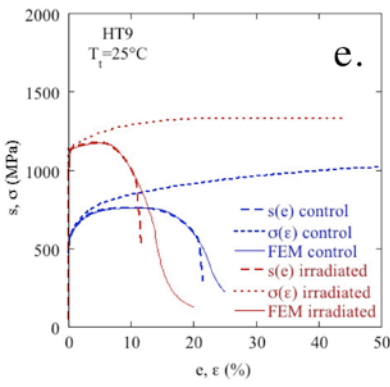
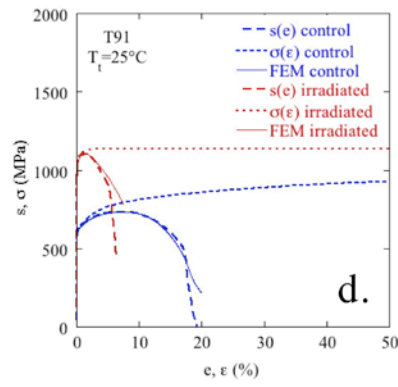
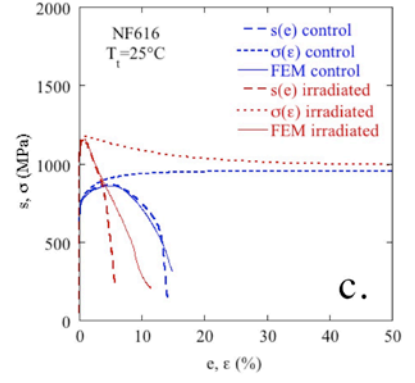
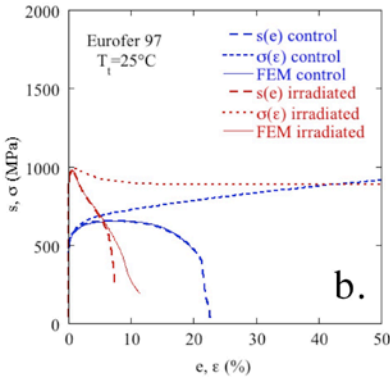
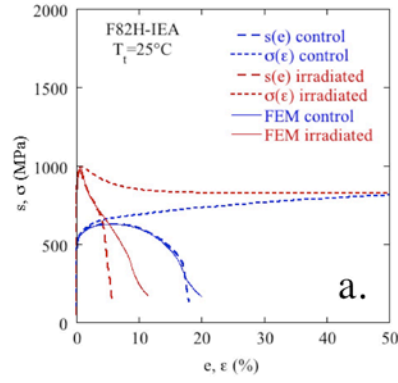
In all cases the unirradiated alloys continuously strain harden, albeit at various rates. However, following irradiation the $\sigma(\epsilon)$ fall into one of three general classes of behavior: i) strain softening up to $\epsilon \approx 10\text{-}20\%$, followed by an approximately constant, perfectly plastic $\sigma(\epsilon)$; ii) a very small range of strain hardening

followed by a constant perfectly plastic $\sigma(\epsilon)$; and iii) continuous strain hardening. For tests at 25°C, type i behavior is observed for F2, E9 and N6, type ii for T1 and type iii for H9 and M7. At 300°C the pattern is similar, but N6 continues to slowly soften up to 50% and the H9 displays type ii behavior. For tests at 25°C the FH, E7 and N6 irradiated $\sigma(\epsilon)_i$ approach the unirradiated $\sigma(\epsilon)_u$ at $\epsilon \approx 50\%$, while the $\sigma(\epsilon)_i$ remains higher for T1, H9 and M7. In the case of the 300°C tests, the $\sigma(\epsilon)_i$ remain significantly higher than the $\sigma(\epsilon)_u$ over the entire strain range examined.

Note, that we have previously carried out a similar analysis of F2 tensile test data from High Flux Isotope Reactor irradiations [14,30]. In the dose range of ≈ 4.9 to 18 dpa at $\approx 300^\circ\text{C}$ and for strains up to 50%, one case showed strain softening, while another was closer to perfectly plastic with slight strain hardening following a nearly perfectly plastic low strain increment with slight softening. However, in a third case, significant, continuous strain hardening was observed after a small increment of perfectly plastic flow. And in all three cases at more than 7 dpa, strain hardening was found at even higher strains. Possible effects of high levels of He, produced in a spallation proton irradiation, on $\sigma(\epsilon)_i$ were also observed. The reasons for the similarities and differences between these previous and current results will be explored in future research.

As noted previously, the plastic strain range between 0 and 10% is especially important since this probably represents a practical structural limit and since this plastic strain range plays a dominant role in both hardness and fracture toughness. Figure 2a and b compare the $\Delta\sigma_y$ and the average flow stress between 0 and 10% ϵ ($\Delta\sigma_{10}$) for all the alloys at both 25 and 300°C, respectively. In general the changes in $\Delta\sigma_{10}$ are less than $\Delta\sigma_y$, with the largest differences for F2, E7 and N6 at 25°C. On average, $\Delta\sigma_{10} \approx 0.78\Delta\sigma_y$ at both test temperatures.

The corresponding yield stress $s_y \approx \sigma_y$ and s_{uts} are summarized in Table 2 both in terms of the absolute values and the irradiation induced changes. Table 2 also summarizes the corresponding ductility data for e_{ui} and e_{ti} . The TMS $\Delta\sigma_y$ vary at 25C from ≈ 540 (H9) to 330 (N6) MPa while the corresponding e_{ui} at 25°C ranges from 4.5 (H9) to 0.61 (F2) %. As more clearly seen in Figure 3a the largest $\Delta\sigma_y$ for tests at 25°C was for H9 followed by T1, E7, N6 and F2. The corresponding $\Delta\sigma_y$ for ODS M7 is much lower than for the TMS alloys. Figure 3b shows the plot of the $\Delta\sigma_y$ versus Δs_{uts} at 25°C. The fit line has a slope of ≈ 0.8 , which is broadly consistent with the author's previous observations.



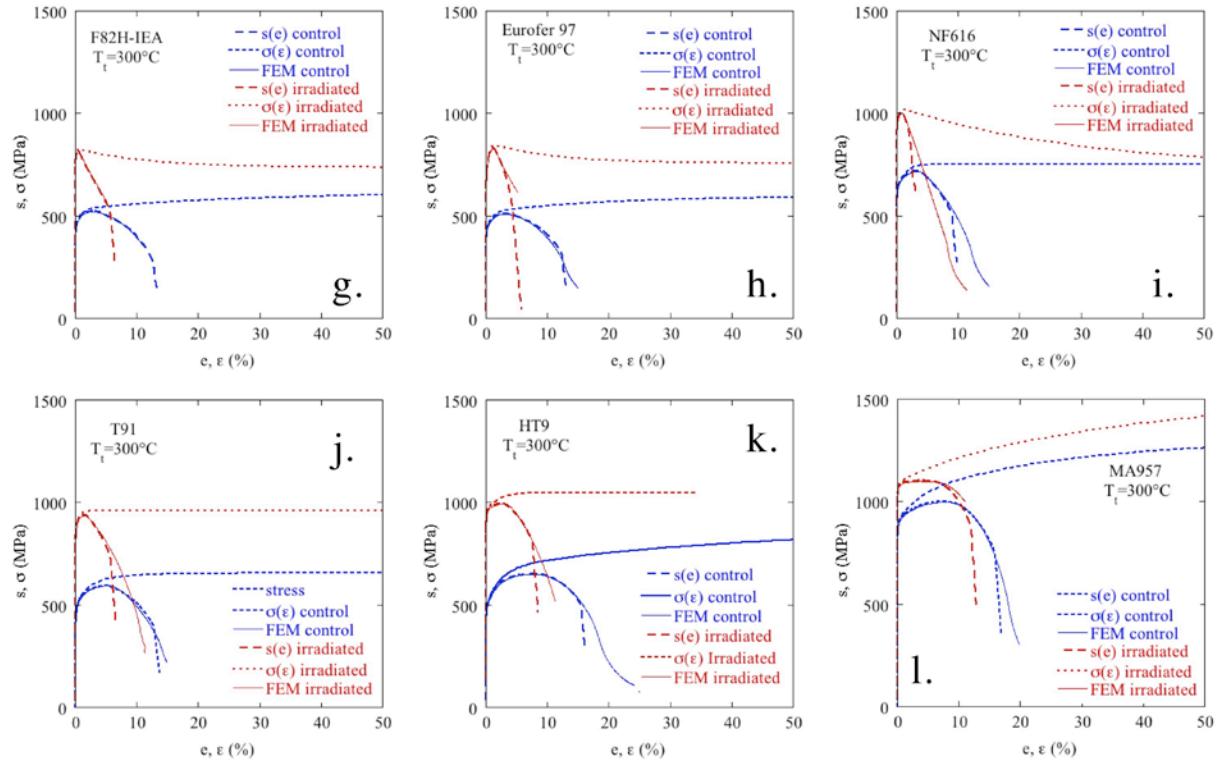


Figure 1 The $s(e)$ curves at 25 and 300°C that were used to derive the corresponding $\sigma(\epsilon)$ constitutive curves using the FEM procedure for the 6 alloys in the unirradiated and irradiated conditions (see text).

Figure 4 shows that all of the irradiated TMS alloys with $\approx 9\text{Cr}$ tested at 25°C have low e_{ui} ($< \approx 1\%$), while the e_u for the 12Cr HT9 alloy is much higher at $\approx 4.54\%$. The highest to lowest e_{ui} ranking for the TMS is $\text{H9} \gg \text{T1} > (\text{slightly}) \text{E7} \approx \text{F2} \approx \text{N6}$. The only difference that is statistically significant is the higher e_{ui} for H9. The unirradiated e_{uu} of H9 is also the highest, but it is not nearly as dissimilar to the e_u for the other lower Cr TMS as in the irradiated condition. Likewise the irradiated total elongation is highest in H9, but is similar for the other alloys. Notably, the post-necking [$e_t - e_u$] ductility is similar in all the TMS averaging $\approx 11.2 \pm 2.2\%$. Thus the effects of irradiation on ductility are mainly to increase hardening and lower strain hardening rates that in combination generally reduce the strains at plastic instability in a tensile test.

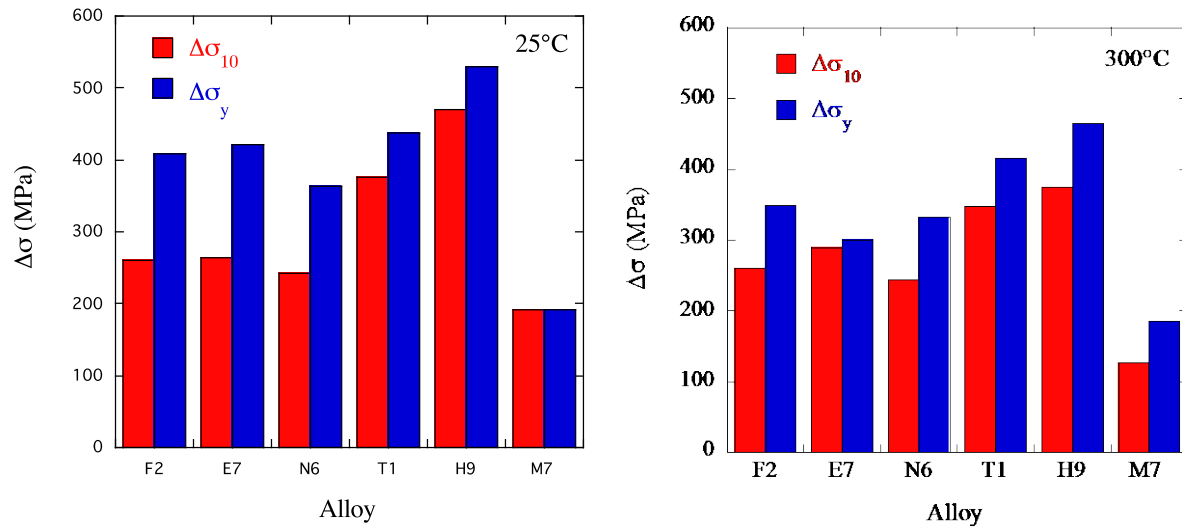


Figure 2. Changes in the average flow stress between 0 and 10% strain ($\Delta\sigma_{10}$) and the corresponding $\Delta\sigma_y$ for tests at: a) 25°C; b) 300°C.

Table 2. Summary of the engineering tensile data

| Alloy | σ_{yu} | s_{uu} | $\Delta\sigma_y$ | Δs_u | e_{uu} | e_{tu} | e_{ui} | e_{ti} |
|-------|---------------|-----------|------------------|--------------|----------|-----------|-----------|-----------|
| H9 | 555/465 | 757/652 | 535/480 | 406/304 | 9.4/8.4 | 21.2/15.6 | 4.0/2.5 | 19.33/7.6 |
| T1 | 610/453 | 730/596 | 420/427 | 360/343 | 6.8/4.8 | 16.9/12.9 | 1.0/1.5 | 4.7/5.8 |
| N6 | 735/630 | 860/719 | 375/330 | 284/284 | 5.4/3.3 | 13.7/9.1 | 0.60/0.68 | 4.3/2.7 |
| F2 | 521/450 | 627/522 | 367/352 | 330/297 | 5.3/2.8 | 17.3/12.7 | 0.60/0.51 | 5.3/5.9 |
| E7 | 528/425 | 651/510 | 397/300 | 313/322 | 6.9/3.0 | 20.3/12.5 | 0.70/2.2 | 6.3/4.2 |
| M7 | 1033/890 | 1178/1002 | 213/180 | 134/102 | 9.9/6.0 | 19.9/16.0 | 6.1/3.6 | 14/12.0 |

The xxx/yyy format indicates data at 25/300°C. Units: stress (MPa), strain (%)

Figure 5a shows that the $\Delta\sigma_y$ for 25°C tests tracks those at 300°C with a slope of ≈ 0.9 , which is consistent with previous experience and the ratio of the corresponding shear moduli. As shown in Figure 5b, there is not a fully consistent pattern in the irradiated e_{ui} at 25 versus 300°C. In 4 of the 6 cases the e_{ui} at 300°C are lower and in 2 cases they are higher than at 25°C. An overall fit to $e_{ui}(300^\circ\text{C})$ versus $e_{ui}(25^\circ\text{C})$ gives a higher temperature intercept of 0.66 and a slope of 0.62, suggesting that on average the tensile ductility decreases over this temperature interval, as is the case for the unirradiated condition. However, as seen in Figure 5b, perhaps with the exception of Eurofer97, the overall alloy-to-alloy pattern of irradiated e_{ui} are similar at both test temperatures.

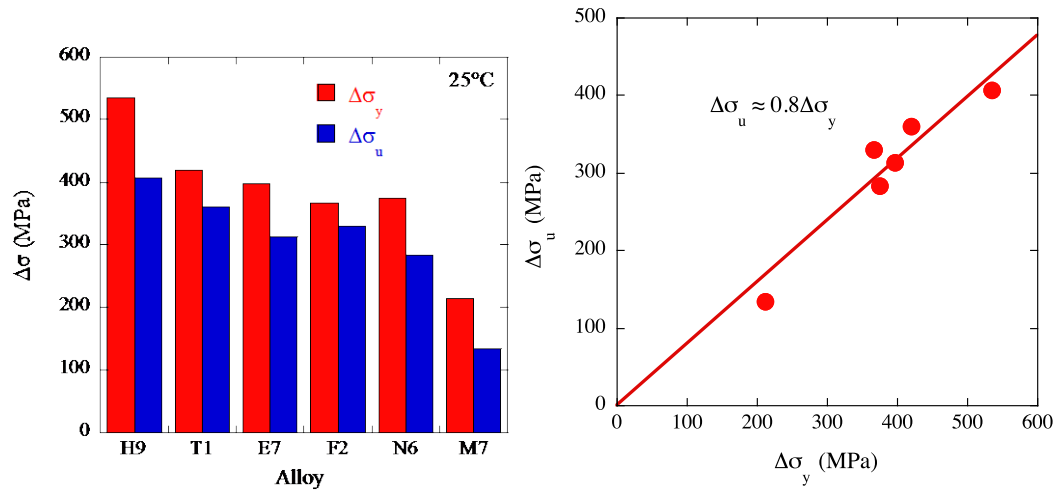


Figure 3. a) $\Delta\sigma_y$ and $\Delta\sigma_u$ for tests at 25°C; b) a plot of the corresponding $\Delta\sigma_y$ versus $\Delta\sigma_u$.

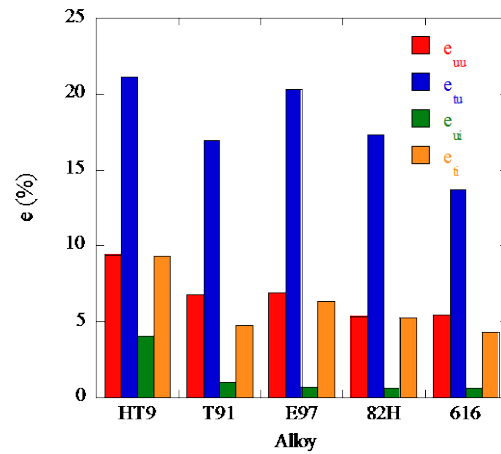


Figure 4. Comparison of the unirradiated and irradiated e_u and e_i for the 5 TMS alloys.

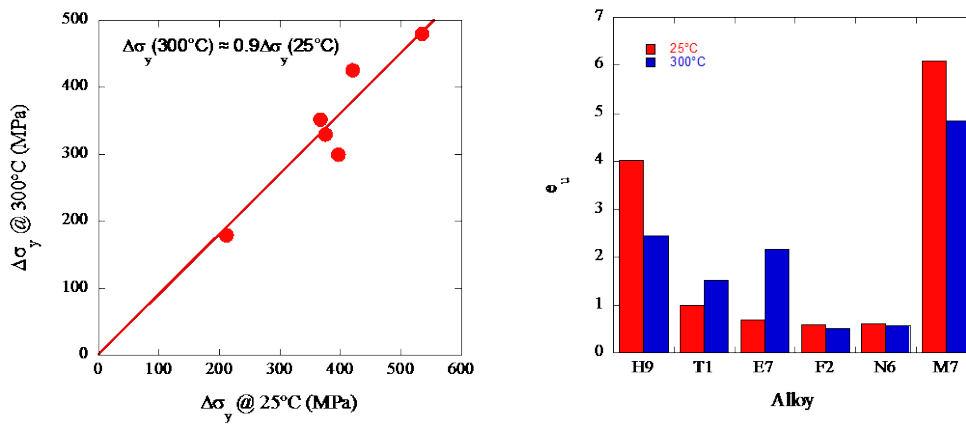


Figure 5. a) $\Delta\sigma_y$ for tests at 300°C versus 25°C; b) e_{ui} at 25 and 300°C.

We have also examined the interrelationships between various tensile properties that will be detailed in future publications for a larger matrix of alloys that includes one austenitic stainless steel and several additional ODS alloys. However, as a preview, Figure 6 shows the variation of the $\Delta\sigma_{yi}$ and $\Delta\sigma_{ui}$ for tests at 25°C, with the corresponding unirradiated σ_y for 11 alloys irradiated in ATR-1. While there is some scatter, the decrease in irradiation hardening, $\Delta\sigma_y$, with increasing unirradiated alloy σ_{yu} is clear and compelling. There are several explanations for this trend, such as strengthening superposition rules [32], but further analysis is beyond the scope of this paper.

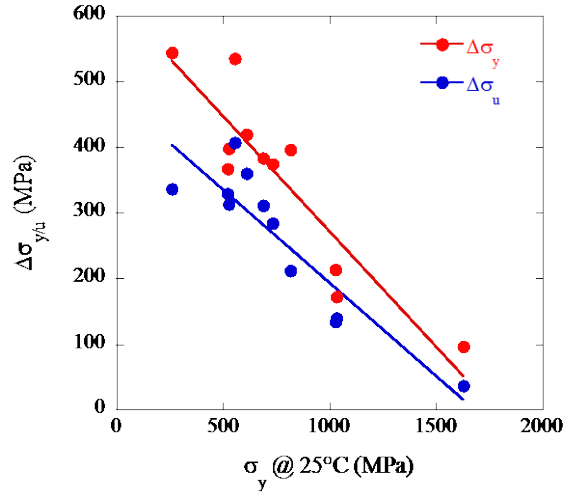


Figure 6. The $\Delta\sigma_y$ and $\Delta\sigma_u$ versus the unirradiated σ_y for tests at 25°C.

The tensile data trends summarized above are generally consistent with previous observations, but provide a degree of quantification that has not been previously reported, as well as some new insights. The exception to these general trends is the higher irradiated e_u of HT9. Previous studies reported lower e_u (< 1%) in other heats of H9 for irradiations at temperatures less than 350°C to similar dpa [3]. Possible reasons for the behavior of H9 are discussed in the following section.

7. Discussion of the Higher Ductility of Irradiated MA-957 and HT-9.

The higher ductility of the MA957 is relatively easy to understand and is largely related to the fine grain size on the order of a μm or less. The fine grains both result in higher strain hardening rates due to the higher generation rate of dislocations due to the limited slip length concentrating forest sources and generating geometrically necessary dislocations which also scale with the inverse of the grain size. Further MA957 contains subgrain and matrix features that can enhance dislocation multiplication like strong precipitates that act as bowing sources. Further the fine grains limit the length and propagation of nascent localized shear bands.

There may be similar microstructurally based contributions to the higher strain hardening and uniform strain ductility in the new heat of HT-9. The increase in yield stress after irradiation and reduced loss of ductility may be from different defect-dislocation interactions which may explain why hardening was observed similar to previous irradiations while uniform elongation was retained. Unfortunately, the

unirradiated and irradiated microstructures of this alloy remain to be characterized. This will be explored in future work, which will include studies of the deformed microstructures as well.

There is another possible contributing factor. As noted above, low temperature ductility in ferritic/martensitic steels is affected by localized flow. Previous research has shown that localized flow in ferritic alloys is very sensitive to the free carbon (C) and nitrogen (N) content. For example, C and N content are widely known to affect Luder's band formation [33, 34]. In research by Liu et al. [33], a high purity Fe-17Cr ferritic steel alloyed with Nb was tested after a slow and rapid cooling heat treatments. Slow cooling allows the Nb to form carbides and nitrides, thus removing C and N interstitials from solution. Yield drops and Luder's bands were observed in the rapidly cooled condition, while smooth and uniform yielding was observed in the slow cooled condition. Further, it has been long known that the mechanical properties (e.g. impact strength and toughness) of Fe-Cr alloys are also strongly affected by C and N in solution [27, 35]. More recently, interstitial free ferritic steels have been developed, in large part because of their improved resistance to localized flow. Examples include super-ferritic alloys such as S44627, S44635 and S44660 where Ti and Nb are added, again to remove N and C from solution. For example, a review by Hoile [36] shows how the R-ratio failure limit (plastic strain ratio of width to thickness directions in a sheet) [37] is improved with additions of Ti or Nb in nearly interstitial free steels. Note that tensile test results in Fig. 1 shows that T1 has the second best uniform elongation after irradiation and this alloy contains the highest amount of Nb (0.63 wt%). In addition to previous research, more recent papers have noted the effects of light elements in Fe such as C effects on dislocation loop evolution[38] and segregation of C at dislocation loops[39]. These observations are examples that demonstrate that free C and N could significantly affect mechanical properties in ferritic steels at low temperatures. Notably, these effects may be preserved in the irradiated condition, and indeed may be further enhanced if large populations of defects, like dislocation loops, trap additional free C and N interstitial solutes.

8. Summary and Conclusions

Tensile test results at 25 and 300°C on five 9-12Cr tempered martensitic steels and one 14Cr oxide dispersion strengthened alloy, that were side-by side irradiated to 6.5 dpa at 295°C in the Advanced Test Reactor (ATR), are reported. The main results and conclusions include:

- The irradiated $\sigma(\epsilon)$ laws for these alloys, derived from engineering stress strain curves fall into categories of: strain softening, nearly perfectly plastic and strain hardening.
- Significant variations in $\Delta\sigma_y$ and reductions e_{ui} are observed, where the e_{ui} trends can be understood in terms of the alloy's $\sigma(\epsilon)$ behavior.
- Differences in the average $\sigma(\epsilon)$ increases in the range of 0-10% strain are smaller than the corresponding $\Delta\sigma_y$, and vary more from alloy to alloy. This has important implications to irradiated properties like fracture toughness.
- The observed relation of $\Delta\sigma_{10} \approx 0.8\Delta\sigma_y$ is consistent with previous observations.
- The observed relation of $\Delta\sigma_y(300^\circ\text{C}) \approx 0.9\Delta\sigma_y(25^\circ\text{C})$ is consistent with previous observations.
- The observed decrease in $\Delta\sigma_u$ and $\Delta\sigma_y$ with increases in σ_{yu} is not unexpected, but has not been fully analyzed.

- In five out of six cases the effects of irradiation are generally consistent with previous observations. However, the particular heat of the 12Cr HT-9 tempered martensitic steel in this study has a much higher e_u than observed for earlier heats. The reasons for this behavior are not understood and may be microstructural in origin.
- However, it is noted that the new heat of HT-9, procured under modern quality assurance standards, has lower interstitial free N than previous heats. Notably, there is a general relation between lower interstitial solute contents and improved ductility, and homogenous deformation, in broadly similar steels.

References

- [1] S.A. Maloy, M. Toloczko, J. Cole, T.S. Byun, *Journal of Nuclear Materials*, **415** (2011) 302-305.
- [2] J.L. Straalsund, R.W. Powell, B.A. Chin, *Journal of Nuclear Materials*, **108-109** (1982) 299-305.
- [3] O. Anderoglu, T.S. Byun, M. Toloczko, S.A. Maloy, *Metallurgical and Materials Transactions A-Physical Metallurgy and Materials Science*, **44A** (2013) S70-S83.
- [4] G.R. Odette, *Journal of Nuclear Materials*, **155** (1988) 921-927.
- [5] G.R. Odette, M.J. Alinger, B.D. Wirth, *Recent developments in irradiation-resistant steels, Annual Review of Materials Research, Annual Reviews, Palo Alto, 2008*, pp. 471-503.
- [6] Y. Dai, G.R. Odette, T. Yamamoto, *The Effects of Helium In Irradiated Structural Alloys*, in: Elsevier (Ed.) *Comprehensive Nuclear Materials 1*, 2012.
- [7] M.B. Toloczko, F.A. Garner, C.R. Eiholzer, *Journal of Nuclear Materials*, **212** (1994) 604-607.
- [8] T. Yamamoto, Y. Wu, G.R. Odette, K. Yabuuchi, S. Kondo, A. Kimura, *Journal of Nuclear Materials*, **449** (2014) 190-199.
- [9] G.R. Odette, P. Miao, D.J. Edwards, T. Yamamoto, R.J. Kurtz, H. Tanigawa, *Journal of Nuclear Materials*, **417** (2011) 1001-1004.
- [10] T. Yamamoto, G.R. Odette, H. Kishimoto, J.W. Rensman, P. Miao, *Journal of Nuclear Materials*, **356** (2006) 27-49.
- [11] J. Henry, X. Averty, A. Alamo, *Journal of Nuclear Materials*, **417** (2011) 99-103.
- [12] B. van der Schaaf, C. Petersen, Y. De Carlan, J.W. Rensman, E. Gaganidze, X. Averty, *Journal of Nuclear Materials*, **386-88** (2009) 236-240.
- [13] R.J. Kurtz, A. Alamo, E. Lucon, Q. Huang, S. Jitsukawa, A. Kimura, R.L. Klueh, G.R. Odette, C. Petersen, M.A. Sokolov, P. Spätig, J.W. Rensman, *Journal of Nuclear Materials*, **386-88** (2009) 411-417.
- [14] T. Yamamoto, G.R. Odette, M.A. Sokolov, *Journal of Nuclear Materials*, **417** (2011) 115-119.
- [15] G.R. Odette, T. Yamamoto, H.J. Rathbun, M.Y. He, M.L. Hribernik, J.W. Rensman, *Journal of Nuclear Materials*, **323** (2003) 313-340.
- [16] G.R. Odette, H.J. Rathbun, M. Hribernik, T. Yamamoto, M. He, P. Spatig, *Materials Issues for Generation IV Systems: Status, Open Questions and Challenges, Proceedings of the NATO ASI Science for Peace and Security Series B: Physics and Biophysics, Springer (2008)*, p. 203.
- [17] G.R. Odette, M.Y. He, T. Yamamoto, *Journal of Nuclear Materials*, **367** (2007) 561-567.
- [18] G.R. Odette, M.Y. He, *Journal of Nuclear Materials*, **307** (2002) 1624-1628.
- [19] H.J. Rathbun, G.R. Odette, T. Yamamoto, G.E. Lucas, *Engineering Fracture Mechanics*, **73** (2006) 134-158.
- [20] H.J. Rathbun, G.R. Odette, M.Y. He, T. Yamamoto, *Engineering Fracture Mechanics*, **73** (2006) 2723-2747.
- [21] T.S. Byun, N. Hashimoto, K. Farrell, E.H. Lee, *Journal of Nuclear Materials*, **349** (2006) 251-264.
- [22] M. Victoria, N. Baluc, C. Bailat, Y. Dai, M.I. Luppó, R. Schäublin, B.N. Singh, *Journal of Nuclear Materials*, **276** (2000) 114-122.

- [23] G.R. Odette, M.Y. He, E.G. Donahue, P. Spatig, T. Yamamoto, *Journal of Nuclear Materials*, 307 (2002) 171-178.
- [24] G.R. Odette, D.T. Hoelzer, *JOM*, 62 (9) (2010) 84-92.
- [25] G.R. Odette, *JOM*, 66 (2014) 2427-2441.
- [26] K.L. Murty, *Journal of Metals*, 37 (1985) 34-39.
- [27] A. Hishinuma, S. Takaki, K. Abiko, *Phys. Stat. Sol. (a)*, 189 (2002) 69-78.
- [28] N. Cunningham, Y. Wu, D. Klingensmith, G.R. Odette, *Materials Science and Engineering A-Structural Materials Properties Microstructure and Processing*, 613 (2014) 296-305.
- [29] G.R. Odette, T. Yamamoto, B. Sams, D. Klingensmith, N. Cunningham, G. Waches, J.I. Cole, P.E. Murrey, "Summary of the USCB Advanced Test Reactor National Scientific Users Facility Irradiation Experiment," DOE/ER-0313/46 (2009) 79.
- [30] T. Yamamoto, G.R. Odette, Y. Wu, *Fusion Materials Semi-annual Report 7/1/2011 to 12/31/2011*, DOE/ER-0311/51, (2012) 78-84.
- [31] J.W. Kim, T.S. Byun, *Nuclear Engineering and Technology*, 44 (2012) 953-960.
- [32] G.R. Odette, G.E. Lucas, *Radiation Effects and Defects in Solids*, 144 (1998) 189-231.
- [33] Z.Y. Liu, F. Gao, L.Z. Jiang, G.D. Wang, *Materials Science and Engineering A-Structural Materials Properties Microstructure and Processing*, 527 (2010) 3800-3806.
- [34] F. Gao, W. Zhang, Z. Zhang, Z. Liu, G. Wang, *Precipitates and Luders Elongation in Ferritic Stainless Steels Stabilized with Ti and V*, in: J.M. Zeng, T.S. Li, S.J. Ma, Z.Y. Jiang, D.G. Yang (Eds.) *Advanced Engineering Materials*, Pts 1-3(2011) 16-19.
- [35] W.O. Binder, Spendelow jr., H.R. , *Trans. ASM*, 43 (1951) 759-777.
- [36] S. Hoile, *Materials Science and Technology*, 16 (2000) 1079-1093.
- [37] M. Grumbach, G. Pomey, *Sheet Met. Ind.*, 43 (1966) 515-529.
- [38] D. Terentyev, I. Martin-Bragado, *Scripta Materialia*, 97 (2015) 5-8.
- [39] D. Terentyev, A. Bakaev, E.E. Zhurkin, *Journal of Physics-Condensed Matter*, 26 (2014) 165402.

Acknowledgements

This work at LANL was funded under the Advanced Fuels Campaign of the Department of Energy's (DOE) Fuel Cycle Research and Development Program. The work at UCSB was funded by a DOE NEUP (NU-11-3150) and Office of Fusion Energy Science (DE-FG03-94ER54275) grants. The UCSB ATR-2 irradiations were carried out as part of the National Scientific Users Facility program, with the assistance of a large number of outstanding engineers. The help of Colin Knight in arranging shipment of the specimens from INL to LANL is greatly appreciated. Special thanks also go to UCSB staff members Doug Klingensmith and David Gragg who played the key roles in building the experiment and former PhD student, Dr. Nicholas Cunningham, who carried out the thermal design analysis.